

Genetically Modifying the Protein Matrix of Macroscopic Living Materials to Control Their Structure and Rheological Properties

Jimenez, Esther M.; Nguyen, Carlson; Shakeel, Ahmad; Tesoriero, Robert; Charrier, Marimikel; Stull, Alanna; Ajo-Franklin, Caroline M.

DOI

[10.1021/acssynbio.4c00336](https://doi.org/10.1021/acssynbio.4c00336)

Publication date

2024

Document Version

Final published version

Published in

ACS Synthetic Biology

Citation (APA)

Jimenez, E. M., Nguyen, C., Shakeel, A., Tesoriero, R., Charrier, M., Stull, A., & Ajo-Franklin, C. M. (2024). Genetically Modifying the Protein Matrix of Macroscopic Living Materials to Control Their Structure and Rheological Properties. *ACS Synthetic Biology*, 13(12), 3936-3947. <https://doi.org/10.1021/acssynbio.4c00336>

Important note

To cite this publication, please use the final published version (if applicable). Please check the document version above.

Copyright

Other than for strictly personal use, it is not permitted to download, forward or distribute the text or part of it, without the consent of the author(s) and/or copyright holder(s), unless the work is under an open content license such as Creative Commons.

Takedown policy

Please contact us and provide details if you believe this document breaches copyrights. We will remove access to the work immediately and investigate your claim.

Green Open Access added to TU Delft Institutional Repository

'You share, we take care!' - Taverne project

<https://www.openaccess.nl/en/you-share-we-take-care>

Otherwise as indicated in the copyright section: the publisher is the copyright holder of this work and the author uses the Dutch legislation to make this work public.

Genetically Modifying the Protein Matrix of Macroscopic Living Materials to Control Their Structure and Rheological Properties

Published as part of ACS Synthetic Biology special issue “Materials Design by Synthetic Biology”.

Esther M. Jimenez, Carlson Nguyen, Ahmad Shakeel, Robert Tesoriero, Jr., Marimikel Charrier, Alanna Stull, and Caroline M. Ajo-Franklin*



Cite This: *ACS Synth. Biol.* 2024, 13, 3936–3947



Read Online

ACCESS |



Metrics & More



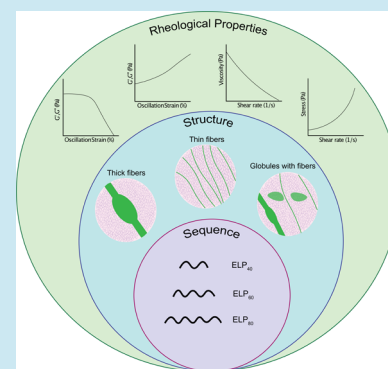
Article Recommendations



Supporting Information

ABSTRACT: The field of engineering living materials (ELMs) seeks to engineer cells to form macroscopic materials with tailorable structures and properties. While the rheological properties of ELMs have been altered using synthetic biology methodology, the relationships connecting their sequence, structural, and rheological properties remain to be elucidated. Recently, our lab created centimeter-scale ELMs from *Caulobacter crescentus* that offer a platform to investigate this paradigm. Here, we explore how changing the elastin-like polypeptide (ELP) length within the protein matrix of this ELM impacts its microstructure and viscoelastic behavior. We demonstrate that shortening ELP produces fibers almost 2× thicker than other variants, resulting in a stiffer material at rest. Interestingly, the midlength ELP forms a complex structure with globules and multidirectional fibers with increased yield stress under flow conditions. Lengthening ELP creates thinner strands between cells with similar storage and loss moduli to those of the midlength ELP. This study begins to elucidate sequence–structure–property relationships in these ELMs and shows that they are complex with few parallels to other biocomposite models. Furthermore, it highlights that fine-tuning genetic sequences can create significant differences in rheological properties, uncovering new design principles of ELMs.

KEYWORDS: engineered living materials, protein matrix, elastin-like polypeptide (ELP), microstructure, rheological properties



INTRODUCTION

Natural living materials, including bone and biofilms, form complex composites made up of an extracellular matrix and living cells that self-assemble and self-organize into hierarchical structures.¹ These structures exhibit remarkable characteristics, such as the ability to maintain themselves over time, and have tunable material properties, which help them thrive in their respective environments.^{2,3} Inspired by these natural materials, the field of engineered living materials (ELMs) aims to develop novel materials based on non-natural combinations of cells and extracellular matrices with tailored functions and properties.^{4,5} Synthetic biologists have focused on introducing biological function into ELMs for a variety of applications, including bioremediation and biomedical purposes.^{6,7}

In contrast to the introduction of biological function, there are only a few examples of using synthetic biology to modify the mechanical properties of ELMs, despite these properties being critical aspects of materials. This is because introducing biological function into an ELM typically requires expressing a soluble intracellular protein, while modifying mechanical properties requires the more complex tasks of expressing, secreting, and directing the assembly of extracellular biomolecules. For example, Ellis and co-workers coexpressed cellulases in ELMs composed of a nanocellulose matrix,

Komagataeibacter rhaeticus, and *Saccharomyces cerevisiae*, decreasing the stiffness of these ELMs.⁵ On the other hand, to stiffen silica biocomposite ELMs produced by *Bacillus subtilis*, Schmidt-Dannert and co-workers coexpressed a cross-linking sequence on the flagella to enhance cell–cell adhesion.⁸ Similarly, Liu and co-workers used antigen–nanobody cross-linking between the extracellular surface of *Escherichia coli* to stiffen bioinks.⁹ While each of these efforts is consistent with prior knowledge from material science on how sequence changes to matrix affect the material properties, none of these studies interrogated how sequence changes affected the structure of the ELM. Without this critical link, sequence–structure–property relationships in ELMs with biologically produced matrices remain untested. This knowledge gap hinders our ability to rationally design ELMs containing biologically produced matrices with desired material properties for real-world applications.^{10,11}

Received: May 11, 2024

Revised: October 18, 2024

Accepted: November 18, 2024

Published: November 27, 2024



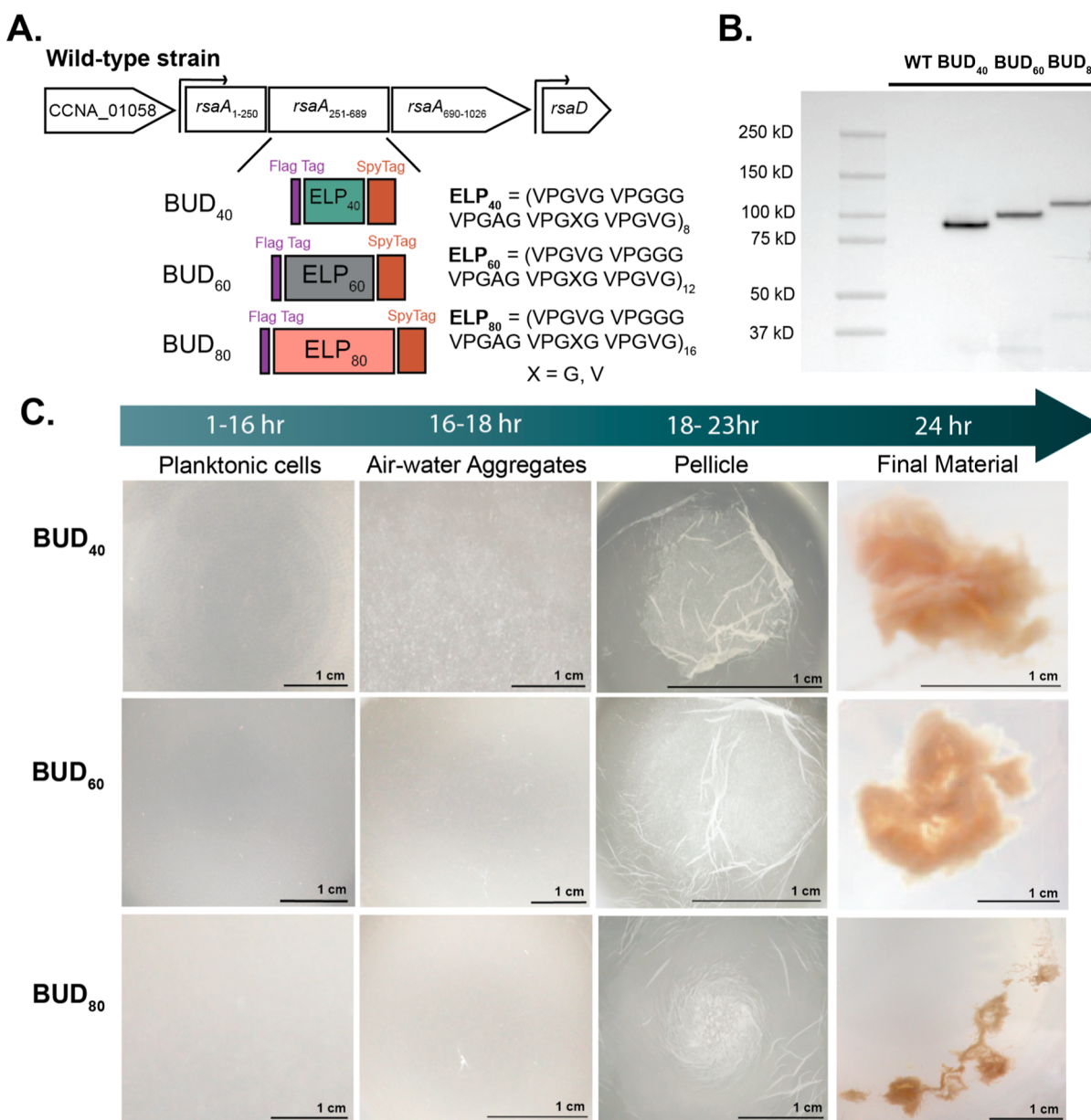


Figure 1. Engineered BUD variant strains assemble into BUD-ELMs. (A) Schematic of the native *rsaA* gene and the constructs encoding the BUD₄₀, BUD₆₀, and BUD₈₀ proteins consisting of *rsaA*_{1–250}, a FLAG-tag, ELP_{*n*}, SpyTag, and *rsaA*_{690–1026}. (B) Immunoblot of culture aliquots using an anti-FLAG-tag antibody showing BUD proteins are expressed and secreted. Lane 2 is Mfm126 labeled WT for “wild-type”, lane 3 is the BUD₄₀ variant, lane 5 is the BUD₆₀ variant, and lane 5 is the BUD₈₀ variant. The culture from the flasks was harvested after 24 h in shaking conditions and was not normalized for total protein. (C) Optical photographs of the BUD₄₀, BUD₆₀, and BUD₈₀ strain cultures during the planktonic stage (first column), the air–water aggregation stage (second column), the pellicle stage (third column), and the fully formed material stage (fourth column). All variants produce BUD protein and yield a total apparent area of 0.2–2 cm².

In comparison to ELMs, sequence–structure–property relationships in protein-based materials are well established. Material scientists have efficiently designed versatile biomaterials composed of proteins such as resilin and elastin to provide multifunctionality and highly tunable features.^{10,12} For example, elastin-like polypeptides (ELPs), synthetic polymers derived from human tropoelastin, demonstrate a significant range of properties from sequence variations. Its consensus sequence (VPGXG)_{*n*} can be manipulated by changing position X to any amino acid other than proline. These mutations alter the physical and rheological properties of the resulting ELP-based materials.^{13,14} Furthermore, studies done in protein-based block copolymers and recombinant protein elastomers

reveal that changing the tandem repeat length results in different rheological properties.^{15,16} Specifically, increasing the tandem repeats in recombinant protein elastomers leads to an increase in tensile strength, a metric describing how much stress the material can withstand before breakage.¹⁶ Although experimental and computational studies have been carried out to understand sequence–structure–property relationships in ELP-based materials, thorough systematic characterization for this paradigm has yet to be done in ELMs, hindering predictive material design.¹⁷

We have recently described macroscopic ELMs composed of a protein matrix and the bacterium *Caulobacter crescentus* that offer a versatile platform for studying sequence–structure–

property relationships. *C. crescentus* has a structurally characterized surface layer (S-layer), RsaA, that can be engineered to ligate materials to its surface,¹⁸ creating a foundation for assembling ELMs. *C. crescentus* can also secrete non-native biopolymers at unprecedentedly high yields¹⁹ to produce a synthetic extracellular protein matrix. Combining these capabilities, we engineered *C. crescentus* to secrete and display a self-associating protein that we termed the BUD (bottom-up de novo) protein. The BUD protein consists of the N-terminus and C-terminus of RsaA, with ELP₆₀ replacing its crystallization domain. This BUD protein is sufficient to cluster cells and form an extracellular matrix, allowing *C. crescentus* to grow into centimeter-size materials called BUD-ELMs.²⁰

Three aspects of BUD-ELMs make them a particularly attractive platform for studying sequence–structure–property relationships. First, the macroscopic size of these materials facilitates their characterization with bulk rheological measurements. Second, the proteinaceous nature of the extracellular matrix makes changing its sequence straightforward, especially compared to that of carbohydrate-based matrices. Third, the rheological properties of the BUD-ELMs can be genetically controlled by a factor of 25× through the deletion of large protein domains in the BUD protein. Taken together, this platform affords the opportunity to understand how fine-tuned changes to the sequence affect the structural and rheological properties of the resulting material for applications.²¹

Here, we explore how fine changes to the BUD protein sequence affect the structural and rheological properties of the resulting BUD-ELMs. We create *C. crescentus* strains expressing BUD proteins with different numbers of ELP tandem repeats and demonstrate that each strain forms distinct BUD-ELMs with different microstructures varying in fiber directionality and thickness. While all the materials have strong shear thinning behavior, shortening the ELP creates a stiffer material, and the midlength BUD-ELM has a higher yield stress. Overall, this study provides insight into how small-scale sequence changes lead to different fibrillar thicknesses and orientations, resulting in a stiffer and stronger material. The novel sequence–structure–property behavior we observe in our materials sheds light on new conceptual models for ELMs, facilitating material design for future applications.

RESULTS

BUD Proteins with Different ELP Repeat Lengths Are Secreted and Self-Assemble into Macroscopic BUD-ELMs. Considerable evidence suggests that increasing the tandem repeats in recombinant ELP elastomers decreases the elastic modulus or stiffness of the material while decreasing the tandem repeats leads to stiffer material.^{15,16} To understand whether this principle is mimicked in de novo living materials, we engineered BUD-ELMs with three different ELP lengths (Figure 1A). We designed variant BUD proteins by replacing the native copy of the S-layer RsaA with a synthetic construct coding four regions using homologous recombination as established in Molinari et al.²⁰ The first domain in these constructs is the surface anchoring domain of RsaA (*rsaA*_{1–250}), allowing monomers to attach to the surface of *C. crescentus*. Following this domain, we inserted a FLAG-tag, a hydrophilic octapeptide tag, to enable BUD protein detection. Next, we encoded an ELP domain: a synthetic biopolymer derived from tropoelastin composed of a repeating pentapeptide sequence (VPGXG), which self-assembles into a flexible polymer structure in isolation.²² We chose this biopolymer

because it is well-studied and can be recombinantly expressed easily.²³ Following the ELP domain is SpyTag, a peptide that forms an irreversible covalent bond to SpyCatcher, its protein partner.²⁴ Since this split protein system is a well-established covalent functional tag and we know it is functional in RsaA, we used it as a functionalization tag.¹⁸ Lastly, the fourth region encoded is the native secretion sequence of RsaA (*rsaA*_{690–1026}), which is known to self-aggregate.²⁵ These variants were derived from a *C. crescentus* parent strain in which the native S-layer associated protease (*sapA*) is replaced by a xylose-inducible *mKate2*.^{18,44} Each variant has a different tandem repeat length of the ELP: 40 repeats, 60 repeats, or 80 repeats of the VPGXG motif, where X is alanine, glycine, or valine.⁴⁰ Meyer and Chilkoti observed that the physical behavior of ELPs is altered by the addition of 30 tandem repeats to the sequence, and we expected this trend would be reflected in the properties of our materials. To assess whether finer-grained effects could be achieved, we lowered the number of tandem repeats to 20.³⁵ We refer to these variant BUD protein-expressing strains of *C. crescentus* as BUD₄₀, BUD₆₀, and BUD₈₀, respectively. The engineered *rsaA* locus of the BUD₄₀, BUD₆₀, and BUD₈₀ strains were sequence verified.

To confirm that the full-length BUD proteins are secreted into the extracellular media, we collected aliquots of culture after growing in shaking conditions for 24 h and probed these aliquots via immunoblotting with an anti-FLAG-tag antibody. Prior work shows that the wild-type (WT) RsaA and the BUD protein migrate higher than their expected molecular weight.^{20,26} Consistent with their results, BUD₆₀ has an observed band at 100 kDa, despite its expected molecular weight of 94 kDa. The immunoblots illustrate that BUD₄₀ has an observed band at 87 kDa, with its expected molecular weight of 78.5 kDa, and BUD₈₀ has an observed band at 108 kDa while its expected molecular weight was 98 kDa (Figure 1B). Altogether, these data qualitatively demonstrate that the variant strains can express and secrete BUD proteins with ELPs of different lengths.

To test whether these variant BUD strains form centimeter-scale macroscopic material, we inoculated single colonies in liquid culture using standard media and growth conditions established by Molinari et al. We observed that the BUD₆₀ grows cells planktonically for 16 h before forming small aggregates at the air–water interface between 16 and 18 h. Following this is the pellicle stage that forms between 18 and 23 h, and last, the material desorbs from the air–water interface at 24 h and sinks as the final material. The BUD₄₀ and BUD₈₀ strains formed material through the same multistep assembly process with slight differences. Notably, BUD₄₀ appeared to form larger microaggregates in the 16–18 h stage than the other BUD variants. Additionally, BUD₄₀ and BUD₈₀ formed pellicles slightly later, between 20 and 23 h, but both formed material by 24 h (Figure 1C). We also probed the planktonic growth of the BUD₄₀, BUD₆₀, BUD₈₀, and WT strains via optical density (OD₆₀₀). All of the strains grow similarly during planktonic growth, i.e., over the first 15 h (Figure S1). However, while the WT continues to grow planktonically, there is a plateau in planktonic growth for the BUD strains. This plateau coincides with the formation of cell-containing structures at the air–water interface, suggesting that significant cell density is at this interface. These data indicate that the different biopolymer lengths can still induce material formation via the same assembly steps, although with slightly different time points in the pellicle stage.

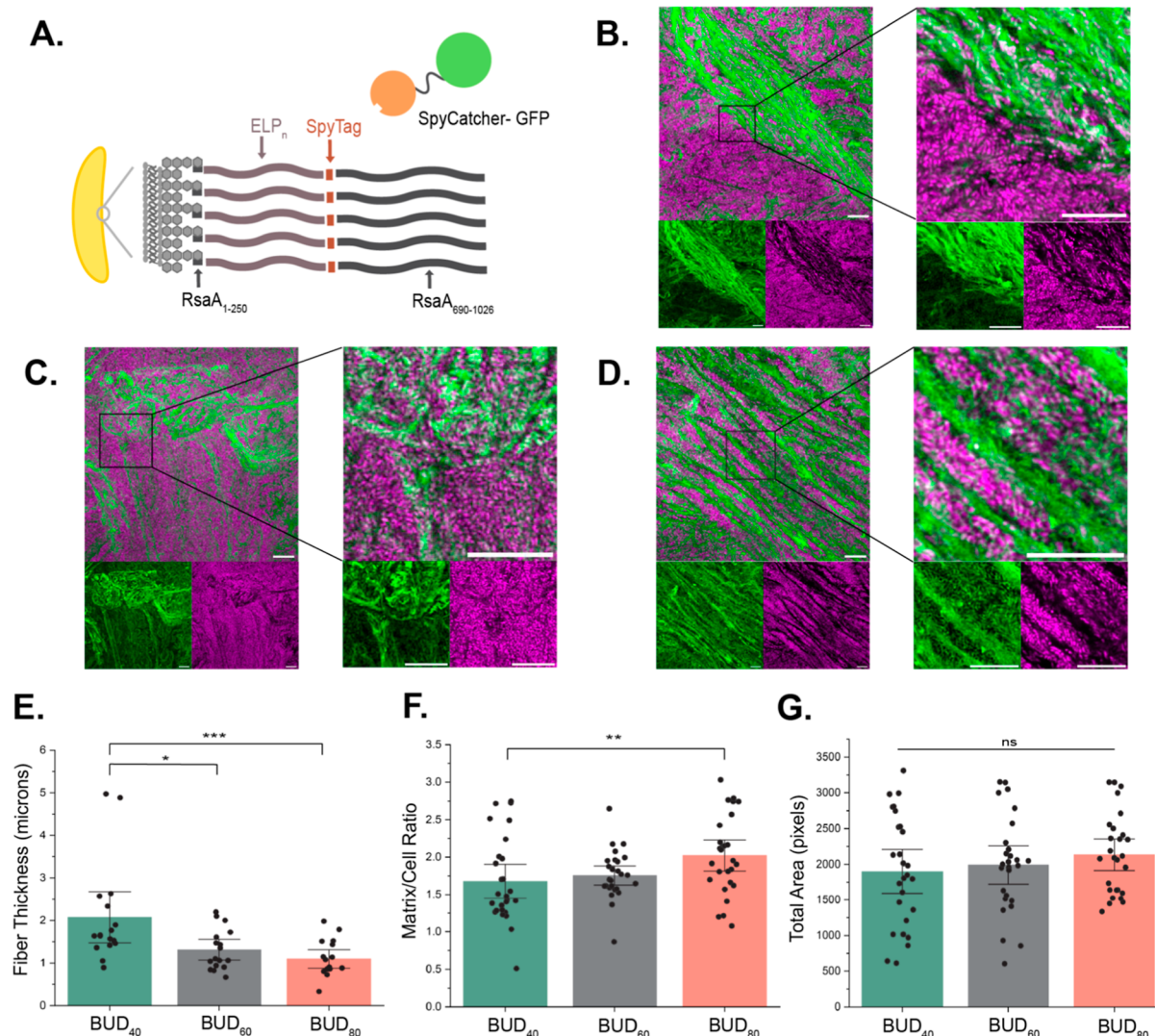


Figure 2. Altering the number of ELP tandem repeats changes the protein matrix microstructure in the BUD-ELMs. (A) Illustration of the redesigned external surface of *C. crescentus* exhibiting RsaA_{1–250}, ELPs of different lengths, SpyTag, and RsaA_{690–1026} attached to the cell's surface and SpyCatcher-GFP linkage to SpyTag. (B–D) Confocal microscopy of (B) BUD₄₀, (C) BUD₆₀, and (D) BUD₈₀ materials with xylose-induced cells producing *mKate2* (magenta) and the BUD protein matrix stained with SpyCatcher-GFP (green). The BUD₄₀ and BUD₈₀ materials contain aligned fibers of protein matrix, while the BUD₆₀ protein matrix is a more complex, globular structure. Scale bars are 10 μm for each image and we imaged 3 biological replicates with 3 fields of view per sample. (E) Comparison of the fiber thickness in microns between the variants showing an increased fiber thickness in the BUD₄₀. Seventeen fibers for each BUD variant were analyzed. (F) Comparison of the matrix/cell ratio between variants distinguishing significant differences between BUD₄₀ and BUD₈₀. We analyzed 3 biological replicates with 3 fields of view. (G) Comparison of the total area in pixels between variants to understand differences in cell clumps. We analyzed 3 biological replicates with 3 fields of view. (*) *p*-value less than or equal to 0.05, (**) *p*-value less than or equal to 0.01, (***) *p*-value less than or equal to 0.001, ns is no significance.

Next, we sought to understand whether the slight differences in material assembly impacted total material production. We found that the differences in assembly did not appear to impact total material production as image analysis of all BUD-ELM variants yielded a total apparent area of 0.2–2 cm² (Figure S2), suggesting similar-sized materials are formed. Interestingly, when removed from the growth flask, the materials appear to retain large amounts of water. To quantify this property, we investigated how much water the materials could hold using thermogravimetric analysis (TGA). These experiments demonstrate that these materials experience a weight loss of 93% (Figure S3A) when heated to 150 °C. This indicates that the materials hold 93% water by mass, and all hold nearly identical amounts of water (Figure S3B). These results reveal that variations in the ELP domain cause modest changes in

assembly timing, but the size of material produced and level of hydration remain the same.

Changing the ELP Length in the BUD Protein Produces Materials with Different Fibrillar Microstructures. Prior research shows that altering the sequence and hydrophobicity of ELP polypeptides affects the resulting microstructure of the material.¹⁶ Thus, we hypothesized that varying the hydrophobicity via the ELP length would impact the microstructure of the variant BUD-ELMs. To investigate this microstructure, we induced intracellular *mKate2* expression before BUD-ELM formation to label the cells, stained the BUD protein matrix after formation using SpyCatcher-GFP,⁴⁵ and visualized both components within the BUD-ELMs with fluorescence confocal microscopy (Figure 2A). When compared to the BUD variants at 24 h, the WT strain showed

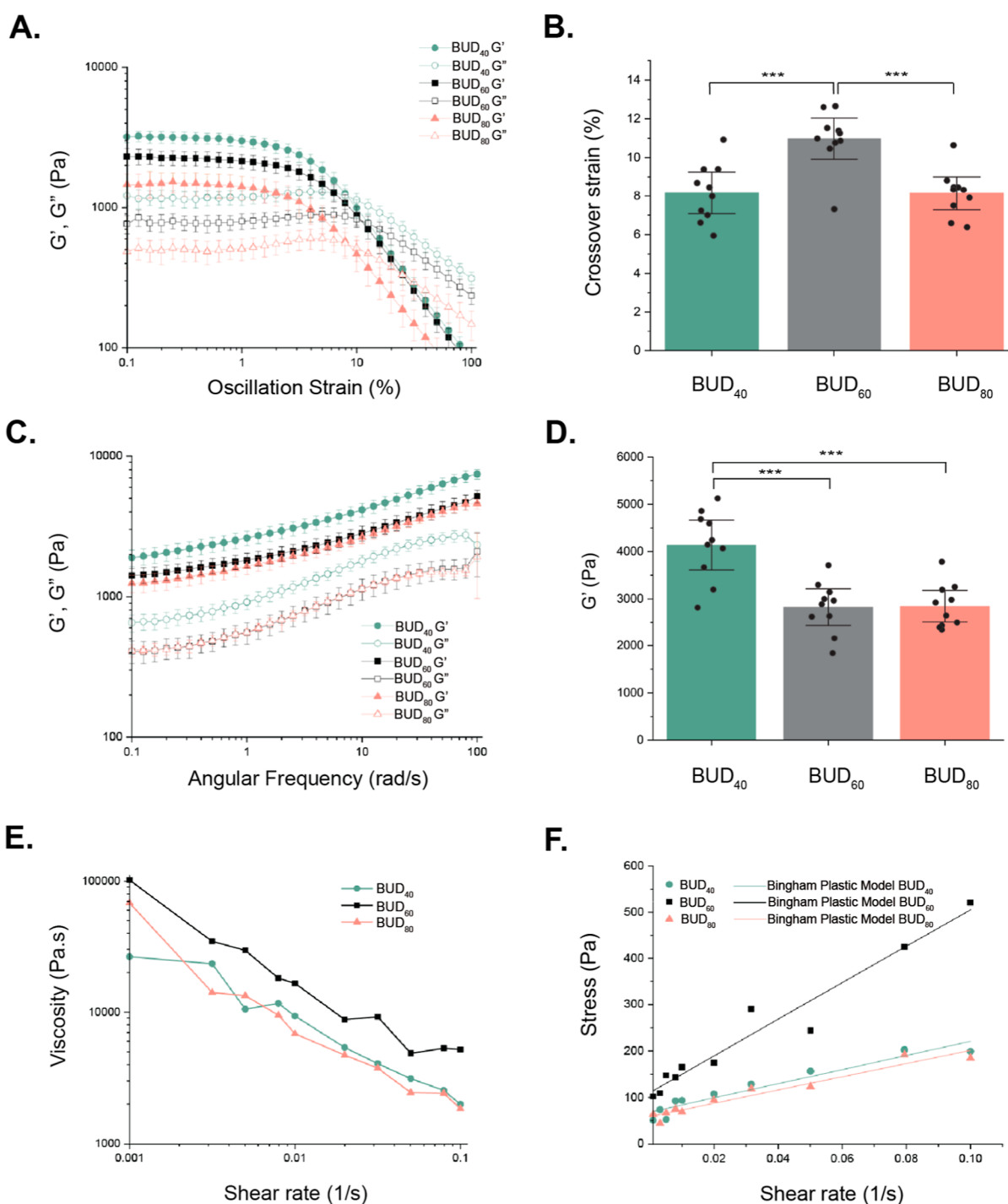


Figure 3. Variant BUD-ELMs have different rheological properties. (A) Oscillation strain sweeps were acquired from 0.1% to 100% strain amplitude at a constant frequency of 3.14 rad/s identifying the linear viscoelastic region of 0.1–1% for the materials. The storage (G') and loss (G'') moduli for BUD₄₀, BUD₆₀, and BUD₈₀ were plotted. (B) The crossover strain (%) of each BUD material was collected from the crossover between G' and G'' . The BUD₆₀ has a higher crossover strain (%), indicating greater resistance to deformation. (C) Frequency sweep measurements were acquired from 0.1 to 100 rad/s at a constant strain amplitude of 1%, demonstrating that BUD₄₀ produces a stiffer material. (D) Average storage (G') modulus of BUD₄₀, BUD₆₀, and BUD₈₀ at an angular frequency of 10 rad/s showing the differences between the stiffness of the materials. Error bars are centered on the mean value and represent 95% confidence intervals of 10 samples. (E) Viscosity vs shear rate of the variants exhibiting strong shear-thinning. (F) Stress vs shear rate of the variants fitted using the Bingham plastic model to compare yield stress values at the y-intercept. The mean value of 2 samples is plotted. (*) p -value less than or equal to 0.05, (**) p -value less than or equal to 0.01, (***) p -value less than or equal to 0.001, ns is no significance.

minor cell clustering likely due to cell–cell adhesion and did not show fiber formation (Figure S4). Most strikingly, we observed different patterns in the BUD protein-containing matrix between variants. BUD₄₀ contains spider web-like

structures that spread between the cells and embed them into the matrix (Figures 2B and SSA). In contrast, BUD₆₀ forms a complex structure consisting of thick and thin fibers surrounded by globular regions of the protein matrix (Figures

2C and S5B). Notably, BUD₈₀ forms thin fiber-like structures surrounded by globular regions of the matrix (Figures 2D and SSC). From the microscopy data, we observed that the fibers in BUD₄₀ and BUD₈₀ appeared to be more tightly aligned in one direction, while the BUD₆₀ appeared to contain randomized fibers with different directions. When we quantified the fiber directionalities in the BUD variants using ImageJ (Figure S6), we found that BUD₆₀ has similar amounts of fibers aligned in all directionalities (Figure S6B). Confirming our visual observations, BUD₄₀ and BUD₈₀ had a higher number of fibers aligned over a 20° range (Figure S6A,C). These findings demonstrate that changing the length of the ELPs in the BUD protein yields changes in the shape and orientation of the protein matrix fibers within the variant BUD-ELMs.

Building upon our understanding of structural differences correlated with three ELP lengths, we investigated fiber thickness in the variant BUD protein matrices. To determine if the fibers formed by the matrix vary significantly in width, we analyzed the confocal microscopy images using ImageJ. As a result, we found that the BUD₄₀ material produces fibers that are, on average, $2.07 \pm 0.56 \mu\text{m}$ thick (Figure S7). In comparison, BUD₆₀ forms fibers about $1.31 \pm 0.23 \mu\text{m}$ thick, and BUD₈₀ forms fibers that are, on average, $1.07 \pm 0.21 \mu\text{m}$ thick (Figures S8 and S9). Statistical analysis using one-way ANOVA followed by the Tukey's honest significant test (HSD) demonstrated a statistically significant difference between the width of the fibers formed by BUD₄₀ and the fibers formed by BUD₆₀ and BUD₈₀ (Figure 2E). This evidence suggests that shortening the length of the ELP produces thicker fibers within the material.

Having established that changing the ELP length affects the microstructure of the materials, we next sought to understand the composition of the materials. To do so, we analyzed the ratio of matrix to cells in each variant material by splitting the image by fluorescent channel and obtaining the average intensity using ImageJ. Our analysis indicated that differences in the matrix/cell ratio are not statistically significant between BUD₄₀ and BUD₆₀ nor between BUD₆₀ and BUD₈₀ (Figure 2F). Conversely, the BUD₈₀ matrix/cell ratio is significantly higher than the BUD₄₀ ratio. To determine whether this increase is due to higher levels of BUD₈₀ protein secretion, we analyzed the amount of protein produced by each strain with an immunoblot. The results show that the band intensities of both the fraction containing intracellular and cell-bound protein and the supernatant fraction for BUD₄₀, BUD₆₀, and BUD₈₀ are not significantly different. This indicates that both the total amount of protein produced and the amount of protein secreted are similar among all three strains (Figure S10A–D). Thus, lengthening ELP in the BUD protein increases the matrix/cell ratio among the strains, but this phenomenon is not due to the protein expression level.

During imaging, we observed several cell-rich regions within all of the variants. Therefore, to establish if the variants differ in overall cell content, we quantified the total cell area present in the confocal microscopy images using ImageJ (Figure 2G). To achieve this goal, we segmented the images to create binary masks of the cell content in each image, from which we measured the total cell area (Figure S11). We found that the total area of cell-rich regions is not statistically significant among the variant materials. This indicates that the amount of cell content within these materials does not differ.

Variant BUD-ELMs Have Different Stiffness and Yield Stress Behavior. Having observed the differences between the material microstructures, we sought to investigate if these changes affect how the materials respond under deformation forces, also known as their rheological behavior.²⁷ Rheological tests enable a material's storage and loss moduli, viscosity, and yield stress to be measured.²⁸ Previous research indicates that decreasing the tandem repeats in purified ELPs leads to stiffer properties, while increasing the number of tandem repeats leads to more flexibility.^{15,16} We hypothesized that this characteristic would be imitated in the BUD-ELMs.

To characterize the rheological behavior of the variant BUD-ELMs, we measured their rheological properties. To keep cells intact in the material, we needed the material to remain hydrated throughout the experiment. To establish the time point at which these materials start to change rheological properties due to dehydration, we conducted standard oscillatory time sweeps on BUD₆₀. The results revealed that the materials' storage modulus started increasing after 20 min on the rheometer, indicating that the material started dehydrating (Figure S12), and therefore, all subsequent tests were carried out within 20 min. Because BUD₆₀ held similar amounts of water as BUD₄₀ and BUD₈₀, we assumed that the dehydration rate would be similar and completed the experiments within 20 min for all samples.

To determine the linear viscoelastic region (LVE) and the crossover point, we performed oscillatory amplitude sweeps. The LVE indicates the oscillation strain range in which frequency sweep tests can be carried out without breaking the polymer network. The crossover point is the oscillation strain (%) where the material transitions from solid-like to liquid-like behavior, represented by storage modulus (G') and loss modulus (G''), respectively. Amplitude sweeps illustrated that the LVE for each variant was between 0.1% and 1% oscillation strain (Figure 3A). Before the 1% oscillation strain, the materials were viscoelastic solid. However, after this threshold, the G' began to decrease, and the materials began to lose their structural integrity, displaying viscoelastic liquid behavior. On an average of 10 replicates, BUD₆₀ has a crossover point of $10.9 \pm 0.74\%$, while BUD₄₀ and BUD₈₀ have lower crossover points, $8.16 \pm 0.94\%$ and $8.14 \pm 0.94\%$, respectively (Figure 3B). Together, these results demonstrate that a higher strain (%) is necessary for BUD₆₀ to flow and exhibit viscoelastic liquid behavior.

As seen in other ELP-based protein systems, we hypothesized that the BUD₄₀ strain would produce a stiffer material because shorter ELP tandem repeats tend to form stiffer materials. To probe G' and G'' , we performed frequency sweeps at a 1% oscillation strain on all three materials. Rheological measurements confirmed that all three variants were viscoelastic solids since G' was significantly higher than G'' (Figure 3C). Additionally, their storage moduli ranged between 1000 and 10,000 Pa. As expected, the frequency curve identified a significantly higher G' and G'' for the BUD₄₀ compared to that for the other variants throughout the angular frequency range of 0.1–100 rad/s (Figure 3C). BUD₆₀ and BUD₈₀ have almost identical G' and G'' values, indicating similar rheological footprint behavior. To present a quantitative comparison between G' of all the materials, we chose values at an angular frequency of 10 rad/s. The results showed that BUD₄₀ G' increases by 1000 Pa compared to BUD₆₀ and BUD₈₀ (Figure 3D). These data suggest that decreasing the tandem repeats of ELP increases the material's stiffness.

Overall, this test demonstrates that through genetic modification of the BUD protein, the change in stiffness of the BUD-ELMs mimics qualitative trends seen in purified ELPs.

Hydrogels are shear-thinning materials because their weak polymer networks break relatively easily under shear stress.²⁹ Given the similarities between BUD-ELMs and hydrogels, we hypothesized these variant BUD-ELMs might be shear-thinning materials.³⁰ To assess this, we employed an equilibrium flow test by applying a constant shear rate until the stress reached equilibrium and analyzed the relationship between the viscosity and shear rate. We observed that the viscosity decreased as the shear rate increased for all three BUD-ELM variants (Figure 3E). Furthermore, when we fitted the data to the power law model, we found that the power law index is similar for all BUD variants (Figure S13). This trend indicates that all the materials show shear-thinning behavior and that changing the number of tandem repeats in ELP does not affect the shear-thinning behavior of the materials.

Next, we wanted to determine the yield stress, the minimum force required to break the material's microstructure at rest to make it flow,³¹ of the BUD-ELM variants. To obtain the yield stress of these materials, we measured the stress as a function of shear rate and fit the resulting trends to the Bingham plastic model³² (Figure 3F)

$$\tau = \tau_0 + \mu_p \dot{\gamma}$$

where τ is the shear stress, τ_0 is the yield point, μ_p is the Bingham viscosity, and $\dot{\gamma}$ is the shear rate. The trends were well-described by this linear relationship, with R^2 for BUD₄₀, BUD₆₀, and BUD₈₀ of 0.92, 0.95, and 0.94, respectively. Because the crossover strain (%) of the BUD₆₀ variant was higher than that of the other variants (Figure 3B), we hypothesized that BUD₆₀ would have a higher yield stress. We found that the yield stress values for BUD₄₀ and BUD₈₀ are very similar, 68.80 ± 7.05 and 59.11 ± 5.69 Pa, respectively (Figure 4A). The yield stress of BUD₆₀ is 110.48 ± 14.1 Pa, which is almost 2 times higher than that of the other materials. The Bingham viscosity follows the same trend as the yield stress, showing that the viscosity of BUD₆₀ at a high shear rate is higher than that of the other variants (Figure 4B). Altogether, these data indicate that under flow conditions, BUD₆₀ exhibits higher yield stress and Bingham viscosity, indicating that these parameters are nonlinearly related to the number of ELP tandem repeats.

DISCUSSION

In summary, our results show that altering the ELP length in BUD-ELMs drives complex, multifaceted changes in the microstructure and rheological properties. Encoding different lengths of ELPs in the BUD protein still produces centimeter-scale BUD-ELMs. Modest alterations in the length of the ELP in the BUD protein vary the orientation and thickness of fibers in the resulting material and their rheological properties. The thicker fibers of BUD₄₀ are correlated with a stiffer material. The randomized complex network of fibers in the BUD₆₀ is associated with a 2× higher yield stress and plastic viscosity compared to the BUD₄₀ and BUD₈₀ variants. This work reveals connections between genetic sequence, fiber morphology, and rheological properties in ELMs that begin to elucidate sequence–structure properties in these emerging materials.

This study suggests that microstructure characteristics are a function of the ELP sequence length in BUD-ELMs. All of the

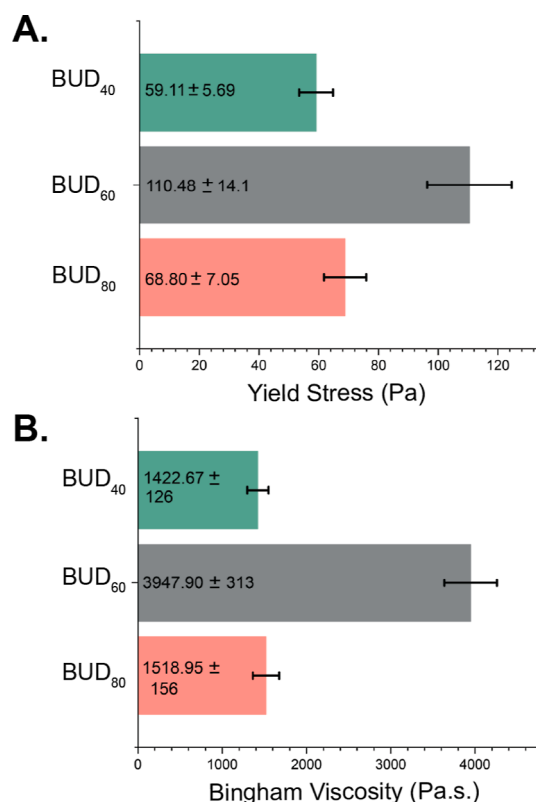


Figure 4. Yield stress and Bingham viscosity for the BUD variants. (A) Average yield stress values for the BUD variants. Consistent with the amplitude sweeps, BUD₆₀ has a higher yield stress. (B) Mean Bingham viscosity for the variants showing higher average values for BUD₆₀. Error bars are centered on the mean value and represent the standard error of 2 technical samples.

variant BUD-ELMs formed fibers in their microstructure. This is consistent with previous work where researchers show that “double-hydrophobic” ELP block copolymers made up of the sequence (VGGVG)₅–(VPGXG)₂₅–(VGGVG)₅ generate nanofibers.³³ Surprisingly, we also see that the thickness of the microfibers is inversely correlated with the length of the ELP: longer ELPs generate thinner fibers. We put forth two possible explanations for this trend. First, the longer ELPs could act as more flexible linkers, decreasing the nucleation of individual fibers and, thus, decreasing their width. A similar phenomenon was observed with silk fibers that nucleated on the surface of *B. subtilis*: silk peptides with less flexible linkers increased nucleation leading to thicker fibers.³⁴ An alternative explanation is that the decreasing fiber thickness arises from the increasing hydrophobicity of the longer ELPs. The sequence of our ELP means that the overall hydrophobicity of the ELP increases as the tandem repeat length increases.³⁵ Thus, the difference in hydrophobicity between these variants may play a role in the fiber formation process. More broadly, the patterns in the fiber microstructure observed in this work cannot be explained by previously reported sequence–structure relationships for existing biomaterials such as resilin, cellulose, or silk. This further demonstrates the need for in-depth characterization of ELMs to develop models. Additional studies are underway to examine the BUD protein assembly process and identify the interactions responsible for the differences in fiber formation.

Our work also suggests that specific microstructure characteristics are connected to certain rheological properties within BUD-ELMs (Figure 5). We observed that BUD₄₀

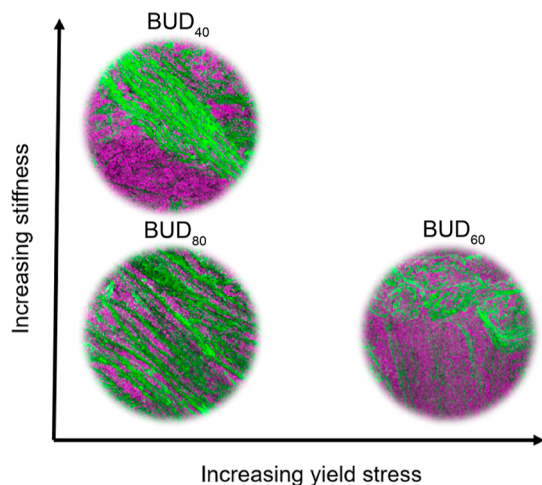


Figure 5. Illustration connecting the sequence–structure–property relationships of the BUD variants. BUD₄₀ produces thicker fibers that contribute to an increased stiffness of the material at resting conditions. Under flow conditions, BUD₆₀ creates a complex structure consisting of matrix globules and nondirectional fibers that help increase its yield stress.

produces stiffer materials at rest compared to BUD₆₀ and BUD₈₀. We suggest this may arise from the thick fibers produced by the matrix. In addition, we found that BUD₄₀ and BUD₈₀ have lower yield stress and plastic viscosity than the BUD₆₀. Hypothetically, this is due to the oscillation shear stress being imposed in a direction parallel to the fiber alignment (fibers aligned in the direction of shear), causing the strength exerted by the fibers to be lower than if the stress was imposed in the perpendicular direction as seen in cellulose nanofibers.³⁶ We do not know the direction in which the fibers are aligned in the material during rheological measurements; therefore, we cannot control the direction of the stress with the fibers. In contrast, BUD₆₀ has a complex, randomized microstructure, where the fibers are aligned in various directions, achieving resistance to flow in different directions and causing the material to be high strength.³⁷

Taken together, this study advances our insight into sequence–structure–property relationships in three ways. The first insight is an increased understanding of the rheological behavior of these BUD-ELMs. This work enabled us to identify these BUD-ELMs as shear-thinning materials that could be applied to biomedical applications, such as drug delivery and 3D printing.^{38,39} The second advancement is that we established methods to comprehensively characterize the macroscopic, microscopic, and rheological properties of these biomaterials. Third, we obtained insight into how changes to the primary sequence of these proteins create drastic changes in the properties of the materials.

With these insights in hand, forthcoming research should focus on uncovering the diversity of sequences that can self-assemble into ELMs and the relationship among biopolymer sequence length, fiber thickness, and fiber alignment. We envision creating a database of biopolymers that can be swapped into BUD-ELMs to target desired properties such as durability and elasticity for applications in energy, the

environment, and medicine. Additionally, because this work emphasized that small-scale sequence changes can fine-tune the structural and rheological properties of de novo biomaterials, we see future work is needed to develop new conceptual models for resulting emergent properties in BUD-ELMs.

CONCLUSIONS

Understanding sequence–structure–property relationships in ELMs will enable their properties to be predictively designed. Here, we used synthetic biology to investigate these relationships in ELMs with a protein-based matrix. Our results show that in BUD-ELMs, a randomized fiber network allows for resistant behavior in flow conditions, while thick fibers help stiffen the material in rest conditions. This is the first example in biomaterials where thicker fibers produce stiffer materials. We envision these insights paving the way for future applications of these BUD-ELMs in 3D printing new living devices,⁴¹ drug delivery,⁴² and tissue engineering.⁴³ We also see that the new design principles for BUD-ELMs are an opening toward the ultimate goal of predictive design.

METHODS

Construction of Variant BUD-ELM Strains. To generate the variant BUD-ELM strains (BUD₄₀-gCAF018 and BUD₈₀-gCAF019) from the wild-type (Mfm126), we modified the pNPTS138-based integration vector pSMCAF008, which was used to build the original BUD-ELM strain established by Molinari et al. in 2022. By replacing the ELP₆₀ sequence from pSMCAF008 with two in-frame BsaI sites, we created a universal backbone for BUD-ELM constructs (pBTCAF008). The sequences for ELP₄₀, ELP₈₀, and SpyTag were then inserted into this backbone by Golden Gate Assembly. All ELP sequences were obtained from GenScript, and the SpyTag sequence was obtained from Twist Bioscience. The full sequences are found in the [Supporting Information](#).

To generate the variant BUD-ELM strains, plasmids pCAF216 (BUD₄₀) and pCAF215 (BUD₈₀) were first electroporated into *C. crescentus* NA1000 Δ sapA::Pxyl-mKate2 (Mfm126). The culture was then plated on PYE with 25 μ g/mL kanamycin to select for integration of the plasmid. Successful integrants were grown overnight at 30 °C in 2 mL of liquid PYE without selection to allow for recombination. Then, 50 μ L of each culture was plated on PYE and 3% sucrose to select against cells possessing the *sacB* gene, allowing for successful isolation of cells with the correct BUD-ELM genotype. Successful integration of the sequences was confirmed using touchdown PCR with annealing temperature ranging from 72 to 62 °C, decreasing 1 °C per cycle, and the PCR amplifications were sequenced using GENEWIZ. All the strains and plasmids generated in this study are found in [Tables S1 and S2](#).

Growth Conditions of BUD-ELMs. The BUD-ELMs were grown by inoculating a colony of the *C. crescentus* strains into 80 mL of PYE in a 250 mL glass flask. The cultures were grown in an incubator at 30 °C at 250 rpm with a 2 in.-orbit for 24 h.

OD Growth Curve of BUD-ELMs. Small cultures of the WT strain and BUD-ELMs were grown overnight at 30 °C. The starting OD₆₀₀ was normalized and transferred to a 250 mL flask, where the strains were grown in standard conditions over 36 h. Every hour, the OD₆₀₀ was taken on the TECAN Spark plate reader by transferring 150 μ L of culture from the

flask into Costar black flat 96-well plates. PYE was used as a blank, and three flasks were grown for each group.

Immunoblot Analysis of BUD Proteins. Cultures of *C. crescentus* of BUD-ELM strains (gCAF018, RCC002, and gCAF019) were grown in shaking conditions for 24 h. Then, 1 mL of supernatant was taken from each culture flask and diluted with 2× Laemmli buffer, which was loaded onto a TGX Stain Free gel (Bio-Rad Laboratories). After running, the gel was transferred to a 0.2 μM nitrocellulose membrane, left on the bench to dry for 30 min, and then blocked for 1 h at room temperature with SuperBlock Blocking Buffer (Thermo Scientific). Membranes were then washed five times in Tris-buffered saline with 0.1% Tween (TBST) buffer and then incubated in a 1:5000 dilution of monoclonal anti-FLAG antibody for 1 h at room temperature. Membranes were washed an additional five times in TBST buffer. Then, Clarity Max Western ECL Substrate (Bio-Rad Laboratories) was added to the membrane, and the membrane was imaged immediately for chemiluminescence. Image analysis was performed using AlphaView software installed in the FluorChem E system.

Immunoblot Analysis for Protein Secretion Analysis. Cultures of *C. crescentus* of BUD-ELM strains (gCAF018, RCC002, and gCAF019) were grown in shaking conditions until they reached 21 h. The OD was taken for each culture and normalized to 1 OD. To separate the pellet from the supernatant, the culture was collected into a 15 mL tube and spun for 15 min at 4000g using the Avanti J-15 R tabletop centrifuge (Beckman Coulter). Then, to concentrate the supernatant until it was 500 μL, the Amicon Ultra-0.5 mL centrifugal filters (MilliporeSigma) were used and spun for 10 min at 14,000g on the Eppendorf 5424 microcentrifuge. The pellet was resuspended with 1 mL of phosphate-buffered saline (PBS). 10 μL portion of the resuspended pellet and concentrated supernatant for each culture was diluted with 2× Laemmli buffer, which was loaded onto a TGX Stain Free gel (Bio-Rad Laboratories). After running, the gel was transferred to a 0.2 μM nitrocellulose membrane, left on the bench to dry for 30 min, and then blocked for 1 h at room temperature with SuperBlock Blocking Buffer (Thermo Scientific). Membranes were then washed five times in TBST buffer and then incubated in a 1:5000 dilution of monoclonal anti-FLAG antibody for 1 h at room temperature. Membranes were washed an additional five times in TBST buffer. Then, Clarity Max Western ECL Substrate (Bio-Rad Laboratories) was added to the membrane, and the membrane was imaged immediately for chemiluminescence. Image analysis was performed using the AlphaView software installed in the FluorChem E system.

Apparent BUD-ELM Size Measure. To elucidate potential size differences between BUD-ELM strains, we grew flasks of each strain under standard conditions before the bottom of each flask was imaged using a Canon EOS 77D camera. Flasks were positioned within a reflective photobox on a clear plastic surface such that the bottom of the flask stood approximately 11.5 cm above the camera lens. These images were separated into RGB channels using MATLAB R2023b. A subset of the blue channel images was then input into the image classification software ilastik (version 1.3.3) as a training set for the autocontext workflow. The first stage of training separated images into three different classifications: Background, Artifact and Sheared Material, and Material. Artifacts and Small Material were defined as remaining scratches and

stains on the flask that might impact analysis as well as small, sheared pieces of material that would lead to systematic overestimations of the material area. The Material group therefore referred to larger, connected pieces of material. The second stage of training distinguished these larger pieces of material from the rest of the image. Both stages of training utilized all 37 features provided within the ilastik workflow (ilastik, version 1.3.3). From the results of the training set, the second stage segmentation masks for all blue channel images were calculated and loaded into MATLAB R2023b. From these masks, the flat area of each piece of material was calculated; to eliminate any remaining artifacts from analysis, only objects possessing an area equal to or greater than 5% of the total area of material for that given flask were utilized. Additionally, for each image, a conversion rate between pixels and square centimeters was determined using the standard flask diameter as a reference point. After conversion, the total area of material per flask, the largest piece of material per flask, and the distribution of material sizes were measured.

Thermogravimetric Analysis of BUD-ELMs. Variant BUD-ELMs (gCAF018, RCC002, and gCAF019) were grown in 80 mL of PYE at 30 °C and a shaking speed of 250 rpm for 24 h. The samples were collected and weighed at around 13.5 mg. They were heated in a high-temperature 70 μL aluminum pan from 25 to 150 °C at a ramp rate of 5 °C/min. TGA experiments were performed using a Mettler Toledo TGA/DSC 3+ STARE System.

Expression and Purification of SpyCatcher-GFP. Single colonies of *E. coli* BL21(DE3) containing plasmids pSMCAF016 for SpyCatcher-GFP expression were inoculated in 25 mL of RM minimal medium with 0.2% w/v glucose and 100 μg/mL ampicillin. The cultures grew for ~16 h at 37 °C and 250 rpm and were then used to inoculate 0.5 L of RM minimal media with 0.2% v/v glycerol, 100 μg/mL ampicillin, and 0.0004% antifoam (Antifoam 204) to a final OD₆₀₀ ~ 0.5. The cultures grew at 37 °C until the mid-log phase and then induced with 0.2% w/v L-arabinose with incubation at 30 °C for ~17 h for protein production.

Cells were harvested by centrifugation at 8000g for 30 min, the pellet resuspended in lysis buffer (50 mM Tris pH 8.0, 300 mM NaCl, 5% v/v glycerol, and 10 mM imidazole) and lysed using Avestin Emulsiflex C3 homogenizer. The lysate was centrifuged at 12,000g for 1 h, and the supernatant was collected for protein purification. The protein was purified using immobilized metal affinity chromatography with a HisTrap FF column and buffers consisting of 50 mM Tris pH 8.0, 300 mM NaCl, 5% v/v glycerol, and 10–250 mM imidazole. Protein purity was confirmed by SDS-PAGE. The purified protein was dialyzed into TEV-cleavage buffer (50 mM Tris pH 8.0, 0.5 mM EDTA, 1 mM DDT), and the 6× His-tag was cleaved using TEV protease with agitation at 4 °C for 4 h. The protein was then stored at –80 °C in 50 mM NaPO₄ pH 8.0, 300 mM NaCl, and 5% v/v glycerol.

Confocal Microscopy. Single colonies of variant BUD-ELM strains (gCAF018, RCC002, and gCAF019) were inoculated in 80 mL of PYE with 0.15% D-xylose to induce the expression of *mKate2*, in a 250 mL flask and grown in 24 h at 30 °C at a shaking speed of 250 rpm. The material was collected and washed twice with 1 mL of 0.01 M PBS in an Eppendorf tube. Then they were incubated with 80 μg/mL of SpyCatcher-GFP for 1 h. After incubation, the samples were washed three times with 1 mL 0.01 M PBS, and then some of the material was placed between a glass coverslip-bottomed 50

mm Petri dish with a glass diameter of 30 mm (MatTek Corporation) and a slab of PYE agarose (1.5% w/v). The Zeiss LSM800 Airyscan confocal microscope was used for imaging. Data were analyzed using ImageJ software.

Matrix/Cell Ratio Analysis. The cell fluorescence intensity for the cells and matrix was analyzed using ImageJ. The intensity of 27 images was averaged for the cells and matrix. The matrix/cell ratio was calculated by dividing the mean intensity for the matrix by the mean intensity for the cells.

Mean fluorescence intensity of matrix (M_{avg})

$$= \frac{M_1 + M_2 + M_3 \dots M_{27}}{27}$$

Mean fluorescence intensity of cells (C_{avg})

$$= \frac{C_1 + C_2 + C_3 \dots C_{27}}{27}$$

$$\text{Matrix cell ratio} = \frac{M_{\text{avg}}}{C_{\text{avg}}}$$

Cell Clump Analysis. We assumed that the more black pixels exposed in the image, the more the cell clumps within the image, and the fewer black pixels in the final image, the fewer the cell clumps in each image. To obtain the total black pixelated area that did not have cells, the threshold was adjusted to highlight the cell clumps in black. Then, a binary mask of this black-and-white image was created to highlight the area that does not have cells in black. The black area was then measured, and an average was taken using the 27 samples.

Rheological Measurements. The variant BUD-ELMs were grown in standard conditions and then collected into a 1.5 mL Eppendorf tube and spun for 10 s at 3200 rcf using a mini centrifuge (VWR-C0803). Then the supernatant was removed, and 200 μL of fresh PYE was added to the BUD-ELMs to prevent the material from getting dry. The rheological properties of the variant BUD-ELMs (gCAF018, RCC002, and gCAF019) were evaluated on a strain-controlled ARES G2 rheometer with a 0.1 rad 8 mm diameter cone plate geometry. Preshearing was performed before each test at a 1% shear rate for 30 s with a 10 s equilibration time. Small amplitude time sweeps were performed for 3600 s at a 0.5% oscillation strain and a fixed frequency of 0.1 rad/s. Strain sweep experiments from 0.1 to 100% oscillation strains were performed at a fixed frequency of 3.14 rad/s. Frequency sweep experiments were conducted at a 1% strain amplitude from 100 to 0.1 rad/s. Equilibrium stress growth tests were performed at constant shear rates of 0.001, 0.00316, 0.00501, 0.00794, 0.01, 0.01996, 0.03163, 0.05013, 0.07944, and 0.1 for each variant until stress equilibrium was reached with a 2% tolerance within 3 consecutive points. These data were further used to get the flow curve, which was plotted as viscosity (Pa·s) vs shear rate (1/s) and shear stress (Pa) vs shear rate (1/s). Data were acquired using TRIOS software (version 4.2.1.36612) and analyzed using Origin (version 9.9.0.225).

■ ASSOCIATED CONTENT

SI Supporting Information

The Supporting Information is available free of charge at <https://pubs.acs.org/doi/10.1021/acssynbio.4c00336>.

Characterization of the size and hydration properties of each material; fibers used for structural analysis, their respective directionalities, and the cell-clump images; confocal microscopy of the WT strain; western blot to compare protein secretion between strains; rheological tests to further characterize the materials; target sequences; and tables of strains and plasmids used in this work. (PDF)

■ AUTHOR INFORMATION

Corresponding Author

Caroline M. Ajo-Franklin – Department of BioSciences, Rice University, Houston, Texas 77005, United States; Department of Chemical and Biomolecular Engineering, Department of Bioengineering, and Rice Synthetic Biology Institute, Rice University, Houston, Texas 77005, United States; orcid.org/0000-0001-8909-6712; Email: cajo-franklin@rice.edu

Authors

Esther M. Jimenez – Department of BioSciences, Rice University, Houston, Texas 77005, United States

Carlson Nguyen – Department of BioSciences, Rice University, Houston, Texas 77005, United States

Ahmad Shakeel – Department of Aerospace Structures and Materials, Delft University of Technology, Delft 2629 HS, Netherlands; orcid.org/0000-0002-0627-7540

Robert Tesoriero, Jr. – Department of BioSciences, Rice University, Houston, Texas 77005, United States

Marimikel Charrier – Department of BioSciences, Rice University, Houston, Texas 77005, United States; orcid.org/0000-0003-4264-5985

Alanna Stull – Department of BioSciences, Rice University, Houston, Texas 77005, United States

Complete contact information is available at: <https://pubs.acs.org/10.1021/acssynbio.4c00336>

Author Contributions

E.M.J.: Conceptualization, funding, investigation, writing—original draft, and writing—review and editing. C.N.: Investigation. A.S.: Formal analysis. R.T., Jr.: Conceptualization. M.C.: Supervision, and writing—review and editing. A.S.: Conceptualization. C.M.A.-F.: Conceptualization, funding, supervision, and writing—review and editing.

Notes

The authors declare no competing financial interest.

■ ACKNOWLEDGMENTS

We thank the Shared Equipment Authority at Rice University for the access to core facilities and instruments, and Alloysius Budi Utama for training. We gratefully acknowledge the financial support of the National Science Foundation Graduate Research Fellowship to E.M.J. (ID 2022300506), CPRIT to C.M.A.-F. (award no. RR1900063), and the Welch Foundation to C.M.A.-F. (award no. C-2130-20230405). We thank our colleagues Dr. Leanne M. Friedrich and Swetha Sridhar for fruitful scientific conversations.

■ REFERENCES

(1) Ashby, M. F.; Gibson, L. J.; Wegst, U.; Olive, R. The mechanical properties of natural materials. I. Material property charts. *Proc. R. Soc. London, Ser. A* 1995, 450, 123–140.

- (2) Yin, W.; Wang, Y.; Liu, L.; He, J. Biofilms: The Microbial "Protective Clothing" in Extreme Environments. *Int. J. Mol. Sci.* **2019**, *20* (14), 3423.
- (3) Nguyen, P. Q.; Courchesne, N.-M. D.; Duraj-Thatte, A.; Praveschotinunt, P.; Joshi, N. S. Engineered Living Materials: Prospects and Challenges for Using Biological Systems to Direct the Assembly of Smart Materials. *Adv. Mater.* **2018**, *30* (19), No. e1704847.
- (4) An, B.; Wang, Y.; Huang, Y.; Wang, X.; Liu, Y.; Xun, D.; Church, G. M.; Dai, Z.; Yi, X.; Tang, T.-C.; Zhong, C. Engineered Living Materials For Sustainability. *Chem. Rev.* **2023**, *123* (5), 2349–2419.
- (5) Gilbert, C.; Tang, T.-C.; Ott, W.; Dorr, B. A.; Shaw, W. M.; Sun, G. L.; Lu, T. K.; Ellis, T. Living Materials with Programmable Functionalities Grown from Engineered Microbial Co-Cultures. *Nat. Mater.* **2021**, *20* (5), 691–700.
- (6) González, L. M.; Mukhitov, N.; Voigt, C. A. Resilient Living Materials Built by Printing Bacterial Spores. *Nat. Chem. Biol.* **2020**, *16* (2), 126–133.
- (7) Xu, L.; Wang, X.; Sun, F.; Cao, Y.; Zhong, C.; Zhang, W.-B. Harnessing Proteins for Engineered Living Materials. *Curr. Opin. Solid State Mater. Sci.* **2021**, *25* (1), 100896.
- (8) Kang, S.-Y.; Pokhrel, A.; Bratsch, S.; Benson, J. J.; Seo, S.-O.; Quin, M. B.; Aksan, A.; Schmidt-Dannert, C. Engineering *Bacillus Subtilis* for the Formation of a Durable Living Biocomposite Material. *Nat. Commun.* **2021**, *12* (1), 7133.
- (9) Chen, B.; Kang, W.; Sun, J.; Zhu, R.; Yu, Y.; Xia, A.; Yu, M.; Wang, M.; Han, J.; Chen, Y.; Teng, L.; Tian, Q.; Yu, Y.; Li, G.; You, L.; Liu, Z.; Dai, Z. Programmable Living Assembly of Materials by Bacterial Adhesion. *Nat. Chem. Biol.* **2022**, *18* (3), 289–294.
- (10) Dooling, L. J.; Tirrell, D. A. Engineering the Dynamic Properties of Protein Networks through Sequence Variation. *ACS Cent. Sci.* **2016**, *2* (11), 812–819.
- (11) Molinari, S.; Tesoriero, R. F.; Ajo-Franklin, C. M. Bottom-up Approaches to Engineered Living Materials: Challenges and Future Directions. *Matter* **2021**, *4* (10), 3095–3120.
- (12) Wei, J.; Xu, L.; Wu, W.-H.; Sun, F.; Zhang, W.-B. Genetically Engineered Materials: Proteins and Beyond. *Sci. China Chem.* **2022**, *65* (3), 486–496.
- (13) Urry, D. W.; Luan, C. H.; Parker, T. M.; Gowda, D. C.; Prasad, K. U.; Reid, M. C.; Safavy, A. Temperature of Polypeptide Inverse Temperature Transition Depends on Mean Residue Hydrophobicity. *J. Am. Chem. Soc.* **1991**, *113* (11), 4346–4348.
- (14) Wright, E. R.; McMillan, R. A.; Cooper, A.; Apkarian, R. P.; Conticello, V. P. Thermoplastic Elastomer Hydrogels via Self-Assembly of an Elastin-Mimetic Triblock Polypeptide. *Adv. Funct. Mater.* **2002**, *12* (2), 149–154.
- (15) Muiznieks, L. D.; Keeley, F. W. Biomechanical Design of Elastic Protein Biomaterials: A Balance of Protein Structure and Conformational Disorder. *ACS Biomater. Sci. Eng.* **2017**, *3* (5), 661–679.
- (16) Nagapudi, K.; Brinkman, W.; Thomas, B. S.; Park, J.; Srinivasarao, M.; Wright, E.; Conticello, V.; Chaikof, E. Viscoelastic and Mechanical Behavior of Recombinant Protein Elastomers. *Biomaterials* **2005**, *26*, 4695–4706.
- (17) López Barreiro, D.; Folch-Fortuny, A.; Muntz, I.; Thies, J. C.; Sagt, C. M. J.; Koenderink, G. H. Sequence Control of the Self-Assembly of Elastin-Like Polypeptides into Hydrogels with Bespoke Viscoelastic and Structural Properties. *Biomacromolecules* **2023**, *24* (1), 489–501.
- (18) Charrier, M.; Li, D.; Mann, V. R.; Yun, L.; Jani, S.; Rad, B.; Cohen, B. E.; Ashby, P. D.; Ryan, K. R.; Ajo-Franklin, C. M. Engineering the S-Layer of *Caulobacter Crescentus* as a Foundation for Stable, High-Density, 2D Living Materials. *ACS Synth. Biol.* **2019**, *8* (1), 181–190.
- (19) Orozco-Hidalgo, M. T.; Charrier, M.; Tjahjono, N.; Tesoriero, R. F.; Li, D.; Molinari, S.; Ryan, K. R.; Ashby, P. D.; Rad, B.; Ajo-Franklin, C. M. Engineering High-Yield Biopolymer Secretion Creates an Extracellular Protein Matrix for Living Materials. *mSystems* **2021**, *6* (2), No. e00903-20.
- (20) Molinari, S.; Tesoriero, R. F.; Li, D.; Sridhar, S.; Cai, R.; Soman, J.; Ryan, K. R.; Ashby, P. D.; Ajo-Franklin, C. M. A de Novo Matrix for Macroscopic Living Materials from Bacteria. *Nat. Commun.* **2022**, *13* (1), 5544.
- (21) Hu, X.; Cebe, P.; Weiss, A. S.; Omenetto, F.; Kaplan, D. L. Protein-Based Composite Materials. *Mater. Today* **2012**, *15* (5), 208–215.
- (22) Riziotis, I. G.; Lamprou, P.; Papachristou, E.; Mantsou, A.; Karolidis, G.; Papi, R.; Choli-Papadopoulou, T. De Novo Synthesis of Elastin-like Polypeptides (ELPs): An Applied Overview on the Current Experimental Techniques. *ACS Biomater. Sci. Eng.* **2021**, *7* (11), 5064–5077.
- (23) Meyer, D. E.; Chilkoti, A. Purification of Recombinant Proteins by Fusion with Thermally-Responsive Polypeptides. *Nat. Biotechnol.* **1999**, *17* (11), 1112–1115.
- (24) Zakeri, B.; Fierer, J. O.; Celik, E.; Chittock, E. C.; Schwarz-Linek, U.; Moy, V. T.; Howarth, M. Peptide Tag Forming a Rapid Covalent Bond to a Protein, through Engineering a Bacterial Adhesin. *Proc. Natl. Acad. Sci. U.S.A.* **2012**, *109* (12), E690–E697.
- (25) Bingle, W. H.; Nomellini, J. F.; Smit, J. Secretion of the *Caulobacter Crescentus* S-Layer Protein: Further Localization of the C-Terminal Secretion Signal and Its Use for Secretion of Recombinant Proteins. *J. Bacteriol.* **2000**, *182* (11), 3298–3301.
- (26) Nomellini, J. F.; Duncan, G.; Dorocicz, I. R.; Smit, J. S-Layer-Mediated Display of the Immunoglobulin G-Binding Domain of Streptococcal Protein G on the Surface of *Caulobacter Crescentus*: Development of an Immunoactive Reagent. *Appl. Environ. Microbiol.* **2007**, *73* (10), 3245–3253.
- (27) Larson, G. R. *The Structure and Rheology of Complex Fluids*; Oxford University Press, 1999.
- (28) Macosko, C. W. *Rheology Principles, Measurements, and Applications*; Wiley-VCH Press, 1994.
- (29) Bashir, S.; Hina, M.; Iqbal, J.; Rajpar, A. H.; Mujtaba, M. A.; Alghamdi, N. A.; Wageh, S.; Ramesh, K.; Ramesh, S. Fundamental Concepts of Hydrogels: Synthesis, Properties, and Their Applications. *Polymers* **2020**, *12* (11), 2702.
- (30) Sathaye, S.; Mbi, A.; Sonmez, C.; Chen, Y.; Blair, D. L.; Schneider, J. P.; Pochan, D. J. Rheology of Peptide- and Protein-Based Physical Hydrogels: Are Everyday Measurements Just Scratching the Surface? *Wiley Interdiscip. Rev.: Nanomed. Nanobiotechnol.* **2015**, *7* (1), 34–68.
- (31) Nguyen, Q. D.; Boger, D. V. Measuring the Flow Properties of Yield Stress Fluids. *Annu. Rev. Fluid. Mech.* **1992**, *24* (1), 47–88.
- (32) Duvaut, G.; Lions, J. L.; John, C. W.; Cowin, S. C. Inequalities in Mechanics and Physics. *J. Appl. Mech.* **1977**, *44*, 364.
- (33) Nagapudi, K.; Brinkman, W. T.; Leisen, J.; Thomas, B. S.; Wright, E. R.; Haller, C.; Wu, X.; Apkarian, R. P.; Conticello, V. P.; Chaikof, E. L. Protein-Based Thermoplastic Elastomers. *Macromolecules* **2005**, *38* (2), 345–354.
- (34) Xie, Q.; On Lee, S.; Vissamsetti, N.; Guo, S.; Johnson, M. E.; Fried, S. D. Secretion-Catalyzed Assembly of Protein Biomaterials on a Bacterial Membrane Surface. *Angew. Chem., Int. Ed.* **2023**, *62* (37), No. e202305178.
- (35) Meyer, D. E.; Chilkoti, A. Quantification of the Effects of Chain Length and Concentration on the Thermal Behavior of Elastin-like Polypeptides. *Biomacromolecules* **2004**, *5* (3), 846–851.
- (36) Li, K.; Clarkson, C. M.; Wang, L.; Liu, Y.; Lamm, M.; Pang, Z.; Zhou, Y.; Qian, J.; Tajvidi, M.; Gardner, D. J.; Tekinalp, H.; Hu, L.; Li, T.; Ragauskas, A. J.; Youngblood, J. P.; Ozcan, S. Alignment of Cellulose Nanofibers: Harnessing Nanoscale Properties to Macroscale Benefits. *ACS Nano* **2021**, *15* (3), 3646–3673.
- (37) Ye, D.; Yang, P.; Lei, X.; Zhang, D.; Li, L.; Chang, C.; Sun, P.; Zhang, L. Robust Anisotropic Cellulose Hydrogels Fabricated via Strong Self-Aggregation Forces for Cardiomyocytes Unidirectional Growth. *Chem. Mater.* **2018**, *30* (15), 5175–5183.
- (38) Purcell, B. P.; Lobb, D.; Charati, M. B.; Dorsey, S. M.; Wade, R. J.; Zellars, K. N.; Doviak, H.; Pettaway, S.; Logdon, C. B.; Shuman, J. A.; Freels, P. D.; Gorman, J. H.; Gorman, R. C.; Spinale, F. G.; Burdick, J. A. Injectable and Bioresponsive Hydrogels for On-Demand

Matrix Metalloproteinase Inhibition. *Nat. Mater.* **2014**, *13* (6), 653–661.

(39) Ouyang, L.; Highley, C. B.; Rodell, C. B.; Sun, W.; Burdick, J. A. 3D Printing of Shear-Thinning Hyaluronic Acid Hydrogels with Secondary Cross-Linking. *ACS Biomater. Sci. Eng.* **2016**, *2* (10), 1743–1751.

(40) Roberts, S.; Dzuricky, M.; Chilkoti, A. Elastin-like Polypeptides as Models of Intrinsically Disordered Proteins. *FEBS Lett.* **2015**, *589* (19PartA), 2477–2486.

(41) Liu, X.; Yuk, H.; Lin, S.; Parada, G. A.; Tang, T.-C.; Tham, E.; de la Fuente-Nunez, C.; Lu, T. K.; Zhao, X. 3D Printing of Living Responsive Materials and Devices. *Adv. Mater.* **2018**, *30* (4), 1704821.

(42) Sankaran, S.; Becker, J.; Wittmann, C.; del Campo, A. Optoregulated Drug Release from an Engineered Living Material: Self-Replenishing Drug Depots for Long-Term, Light-Regulated Delivery. *Small* **2019**, *15* (5), 1804717.

(43) Parra-Torrejón, B.; Jayawarna, V.; Rodrigo-Navarro, A.; Gonzalez-Valdivieso, J.; Dobre, O.; Ramírez-Rodríguez, G. B.; Salmeron-Sanchez, M.; Delgado-López, J. M. Bioinspired Mineralization of Engineered Living Materials to Promote Osteogenic Differentiation. *Biomater. Adv.* **2023**, *154*, 213587.

(44) Shcherbo, D.; Murphy, C. S.; Ermakova, G. V.; Solovieva, E. A.; Chepurmykh, T. V.; Shcheglov, A. S.; Verkhusha, V. V.; Pletnev, V. Z.; Hazelwood, K. L.; Roche, P. M.; Lukyanov, S.; Zaraisky, A. G.; Davidson, M. W.; Chudakov, D. M. Far-Red Fluorescent Tags for Protein Imaging in Living Tissues. *Biochem. J.* **2009**, *418* (3), 567–574.

(45) Pédelacq, J. D.; Cabantous, S.; Tran, T.; Terwilliger, T. C.; Waldo, G. S. Engineering and Characterization of a Superfolder Green Fluorescent Protein. *Nat. Biotechnol.* **2006**, *24* (1), 79–88.